Polytechnic Institute of New York

Route 110

Farmingdale, N. Y. 11735

EXTENDED CONFORMAL MAPPINGS FOR SUPERSONIC AIRCRAFT CALCULATIONS

Semi Annual Progress Report
October 1975 - March 1976

NASA Grant Number NSG-1248

Principal Investigator: Professor Gino Moretti

The NASA Technical Officer for this grant is Mr. Manuel Salas,
NASA Langley Research Center, Hampton, Virginia.

In the first semester of the one-year grant, the following tasks have been performed:

(1) Formulation of a generalized method of conformal mapping to generate computational grids about cross-sections of actual airplanes, including the case of wing cross-sections detached from fuselage cross-sections. The method is entirely analytical and it consists of a repeated application of the Ka'rma'n-Trefftz mapping function. Techniques to make the application of the method automatic have also been developed. The pertinent FORTRAN codes are ready to be used. The analysis has been reported in a paper accepted at the Symposium on Numerical Laboratory Computer Methods in Fluid Mechanics, sponsored by the ASME , in New York, November 1976, and which is reproduced in full in the following pages.

(2) Formulation of the geometry of a sample case, a simplified arrow-wing airplane. A FORTRAN code to generate such a geometry at any number of specified cross-sections and with a variety of basic parameters has been provided to NASA on February, 1976.

(3) Formulation of the gasdynamical analysis of a three-dimensional, supersonic, inviscid, steady, shockless flow past an arbitrary airframe, using the computational grids generated by (1). The analysis, which includes special treatments for body points and bow-shock points, relies on the equations of motion written in terms of logarithm of pressure, entropy and two angles reprising the velocity vector. A FORTRAN code including the sample geometry of (2) has been prepared and is almost totally debugged. To date, the flow analysis is considered reliable wherever the cross-section is elliptic in shape. Further tests are being conducted to determine reliability in more complicated cases. A detailed report on the analysis is in the process of being written and it will be submitted to NASA shortly. Results of the calculations will be submitted for acceptation at the winter meeting of AIAA, January 1977.

CONFORMAL MAPPINGS FOR COMPUTATIONS OF STEADY, THREE-DIMENSIONAL, SUPERSONIC FLOWS

1. Introduction

Steady, supersonic, three-dimensional, inviscid flows can be evaluated numerically by marching techniques, which amount to integrating the equations of motion in successive steps along a fixed axis lying in the general direction of the velocity vectors. In the numerical analysis of the flow about a vehicle, we will stipulate that our basic frame of reference is a Cartesian-(x, y, t) frame, whose t-axis lies along the body and whose (y, t) plane is the plane of symmetry of the body. The symbol t is used here in lieu of the conventional z to avoid confusion with z as a complex variable; the choice of t is suggested by the time-like role which t plays in the numerical procedure. In fact, at each computational step a set of initial values is known at a certain number of points on a plane, normal to the t-axis and a set of final values is to be determined at corresponding points on another plane, also normal to the t-axis, downstream of the initial plane; Δt is the distance between the two planes.

For the sake of accuracy, the following conditions should be satisfied:

1) Computing at evenly spaced grid points;
2) Having a set of grid points exactly on the body and on the outer boundary (the bow shock);
3) Making the grid in each t = constant plane as close as possible to an orthogonal grid, particularly in the vicinity of the body.

The Cartesian frame being obviously unable to satisfy the second condition, it is necessary to recast the equations of motion with reference to another set of independent variables, X, Y and T, such that the X=0

plane represents the body surface and the X=1 plane represents the bow shock wave; in addition, to satisfy the third condition, the two families of X = constant and Y = constant lines in any plane normal to the t-axis should be as close as possible to an orthogonal net, at least in the vicinity of the body.

If the geometry of the rigid boundaries is simple, the mapping can be obtained in a straightforward manner. For example, to study the flow past a nearly circular cone (Fig. 1a), the equations of motion can be written in a cylindrical (ρ, θ, τ) frame, with

$$\begin{aligned} x &= \rho \cos \theta \\ y &= \rho \sin \theta \\ t &= \tau \end{aligned} \tag{1}$$

Let $\rho = b(\theta, \tau)$ be the equation of the body wall and $\rho = c(\theta, \tau)$ be the equation of the bow shock. Then, the transformation

$$\begin{aligned} X &= \frac{\rho - b}{c - b} \\ Y &= \theta \\ T &= \tau \end{aligned} \tag{2}$$

maps the shock layer onto a parallelepiped, a cross section of which is the rectangle shown in Fig. 1b.* In it, the image of the body is a straight segment, AC (X=0), the image of the bow shock is a straight segment, DF (X=1) and AD and CF are symmetry lines ($y = \pm \pi/2$). Lines defined by evenly spaced values of X and Y are shown in both the computational and the physical plane. The equations of motion are, once more, easily

*Stretchings in either one of the X- and Y- directions can be used, if necessary; in which cases Equations (2) are replaced by more complicated expressions. We are not considering such possibilities in the present paper, since our attention is focussed on the part of the mapping problem, so far expressed by (1).

recast in terms of the computational variables, X, Y and T.

Note that , if the cross sections of the body and the bow shock were concentric circles, the grid in the physical plane would be orthogonal, but this is generally not the case. The lack of perfect orthogonality, however, does not impair the accuracy of the results to within reasonable limits.

To maintain accuracy in the computation of the flow about an elliptic cone, with an axis ratio, say, greater than 5, a more sophisticated mapping is needed. In fact, if we proceeded as in the preceding case, the grid in the physical space (shown in Fig. 2a) would be grossly inadequate in the vicinity of the body. Elliptic coordinates should be adopted in each cross section[1], resulting in the grid shown in Fig. 2b.

The construction of such a grid depends on a simple conformal mapping. Let

$$z = x + iy \tag{3}$$

and

$$\zeta = \rho e^{i\theta} \tag{4}$$

be two complex variables, and let

$$z = \frac{h}{2}\left(\zeta + \frac{1}{\zeta}\right) \tag{5}$$

where h is a real number. If A and B are the semi-axes of the ellipse in Fig. 2b, and

$$h = (A^2 - B^2)^{\frac{1}{2}} \tag{6}$$

the ellipse is mapped onto a circle in the ζ-plane, having its center at the origin and a radius, ρ_o, defined by

$$\rho_o = b = \left(\frac{A+B}{A-B}\right)^{\frac{1}{2}} \tag{7}$$

The portion of the z-plane exterior to the ellipse is mapped onto the

portion of the ζ-plane exterior to the circle. Obviously, the image of the shock in the ζ-plane is another closed line (all the more similar to the shock itself the farther it is from the body since, at infinity, z tends to $\frac{h}{2}\zeta$). Let it be called the $\rho = c$ line. Then, one can proceed as before, using (2).

In what follows, I intend to generalize the concept above, by showing:

1) that simple rules can be found to map the portion of a plane exterior to a given rigid body (or bodies) conformally onto the portion of a plane exterior to a nearly circular contour, so that the final (non conformal) mapping described by (2) and illustrated in Fig. 1 can always be applied;

2) that such mappings can be obtained by repeated applications of a single, and rather elementary, analytic function;

3) consequently, that the application can be automatized, without requiring any guesswork by the user;

4) that all derivatives required for the numerical analysis of the flow can also be evaluated analytically and automatically.

A glance at Fig. 3, where two typical cross sections of an airplane are shown, gives an idea of how much bigger the challenge is in dealing with practical applications than in the idealized case of the elliptic cone. It also shows how drastically the contour to be mapped changes from one cross section to another of the same airplane.

2. Numerical Mapping Technique

Obviously, one could solve the conformal mapping problem numerically on each and every cross sectional plane. The physical shock layer could even be conformally mapped directly onto a rectangle, in this way eliminating the second, non-conformal step expressed by (2). In principle, the problem could be solved by simply adding to the equations of motion the two equations:

(8) $$X_x = Y_y \ , \ X_y = - Y_z$$

which assert that the complex variable $Z = X + iY$ is an analytic function of z defined by the condition that the physical boundaries must be mapped onto the sides of the rectangle, as shown in Fig. 1. The feasibility of such an approach has been demonstrated by J.F. Thompson, et al. in a recent paper[2], which contains a host of seemingly successful applications to incompressible flow problems. Any attempt to compare the strictly numerical approach to the one described in the present paper would be premature. A comparison will require a good amount of additional information; definitive data on computational time are not available; neither do we know, at this time, whether the number of grid points needed to solve the mapping problem numerically would be compatible with, or would exceed the minimum number of grid points needed to perform the flow field analysis. For a three-dimensional, compressible flow, the equations are much more complicated than for a two-dimensional, incompressible flow, even if the latter is viscous. The role played by time in the latter and by the time-like variable t in the former is different; more t-dependent terms appear in the latter than in the former. A possible advantage of the present technique may stem from the fact that it defines the mapping and all related derivatives analytically--that is, exactly. Derivatives produced by the gradual variation in the mapping function along the t-axis, as a result of which the physical grid changes whereas the computational grid remains unchanged, are also definable analytically. It may be worthwhile to mention that full-scale computations of three-dimensional, steady, supersonic flows past airplanes using conformal mappings have been performed already[2] without lengthening the computational time by more than a factor of two.

3. Analytical Mapping Technique

As a first step towards constructing a mapping function, we observe that a typical cross section (such as in Fig. 3a) contains a large number of corners and edges. Each sharp angle in a contour (and its symmetrical on the left half plane) is smoothed out by a mapping of the type:

$$\frac{\zeta - 1}{\zeta + 1} = \left(\frac{z - h}{z + h^*}\right)^{\delta} \tag{9}$$

where h is the complex coordinate of the corner or edge in the z-plane, h^* is its conjugate and δ is the inverse of the external angle in multiples of π. In the ζ-plane, $\zeta = \pm 1$ are the images of the two points, $z=h$, $z=-h^*$ but the contour is now smooth at $\zeta = \pm 1$. All other sharp angles on the contour remain unaltered in the ζ-plane. The mapping defined by (9) is, to within a scale factor, the classic Kármán-Trefftz airfoil-generating function. Note also that the function defined by (5), known as a Joukowski mapping, is a particular case of (9) with a real h and $\delta = 1/2$.

The same procedure can obviously be applied iteratively, each time with a different value of h and a different value of δ, until all corners and edges have been eliminated. Since (9) is symmetric with respect to the imaginary axis, the successive contours remain symmetric in the intermediate planes and in the final plane. The final contour is certainly smooth and, in all cases of practical interest considered so far, very close to a circle.

4. Additional Remarks

The greatest difficulty in writing a general purpose code for the repeated application of (9) stems from the multi-valuedness of the arc-tangent and the need for continuity in the mapping, except across the cut running between the branch-points of (9). Note, first, that (9) can be decomposed into two parts:

(10) $$d = \left(\frac{z - h}{z + h^*}\right)^{\delta}$$

(11) $$\zeta = \frac{1 + d}{1 - d}$$

In turn, (10) can be computed in the form,

(12) $$d = \left|\frac{z - h}{z + h^*}\right|^{\delta} \exp\left\{i\delta[\arg(z - h) - \arg(z + h^*)]\right\}$$

Now,

(13) $$\arg(z-h) = \arctan \frac{y-\beta}{x-\alpha} = \theta_M, \quad \arg(z+h^*) = \arctan \frac{y-\beta}{x+\alpha} = \theta_P$$

if

(14) $$h = \alpha + i\beta$$

The angles θ_M and θ_P are shown in Fig. 4 where the heavy line represents a possible cut. It is clear that, as z moves in the right half plane, θ_P varies continuously and it can be correctly defined by standard ATAN functions in Fortran. The case for θ_M is more difficult. So long as z remains to the right of AB, where Real $(z-h) > 0$, the Fortran definition of θ_M is correct. If z enters the region to the left of AB, <u>below</u> the cut, $-\pi$ must be added to θ_M as defined by Fortran; if that happens <u>above</u> the cut, π must be added. In Fig. 5 more extravagant cuts are shown. In addition to the regions, similar to the ones discussed above, where $\pm\pi$ should be added to θ_M, there are two possible regions, shadowed in the figure, where $\pm 2\pi$ should be added, in order to assure continuity in θ_M. In coding, the difficulty can be circumvented very easily, by introducing a factor, μ, equal to 1 for all points above the cut and to -1 for all points below the cut. If θ_M^o is the value of arctan $[(y-\beta)/(x-\alpha)]$ as provided by Fortran,

$$(15) \qquad \theta_M = \begin{cases} \theta_M^\circ & , \text{ Real } (z-h) > 0, \ \text{sgn}\mu = \text{sgn}[\text{Imag}(z-h)] \\ \theta_M^\circ + \mu\pi & , \text{ Real } (z-h) < 0 \\ \theta_M^\circ + 2\mu\pi & , \text{ Real } (z-h) > 0, \ \text{sgn}\mu \neq \text{sgn}[\text{Imag}(z-h)] \end{cases}$$

The concepts of "above the cut" and "below the cut" are invariant by conformal mapping; therefore, the value of μ for a given point with respect to a given cut need be defined only once even when a string of intermediate mappings is used; this can be done, thus, in either one of two planes where the definition is simple, that is, either on the z-plane or on the final ζ-plane (the plane of the near-circle). In Fig. 6, for example, the cuts needed in the successive intermediate mappings which transform the shape of Fig. 3a into a near-circle are shown, both in the z-plane and in the ζ-plane. The definition of the factors μ in the ζ-plane is obvious.

In principle, the intermediate mappings can be executed in any order. In practice, the coding turns out to be much simpler (and, in many cases, the contour in the ζ-plane closer to a circle) if the edges and corners are eliminated, beginning with the one having the smallest value of δ (largest angle) and in the order of increasing δ's. For example, in the case of Fig. 6, if the corner at D were eliminated before eliminating the edge at E, the corner at F would disappear simultaneously and a special logic should be provided to take care of such a possibility. If the edge at E is eliminated first, F and D are far apart from each other in the following steps and can be treated as usual. An even more delicate situation would arise for a cross section of the type shown in Fig. 7, unless the edge at B is eliminated before treating the corners at A and C. Indeed, if the corner at A (having an exterior angle equal to $\pi/3$) were to be eliminated first, part of the shock layer would penetrate into a second

Riemann sheet (due to the fact that $\delta = 3$) and should be recalled back when treating C. It is clear, instead, that ordering the edges and corners by increasing values of δ results in a simple logical operation.

To conclude our general considerations, let it be noted that, whether we want to proceed from the z-plane to the ζ-plane or vice versa, the nature of the intermediate mappings is the same. In fact (9) can be written as follows:

$$\frac{z - h}{z + h^*} = \left(\frac{\zeta - 1}{\zeta + 1}\right)^{1/\delta} \tag{16}$$

and (16) can be used to obtain z from ζ as (9) was used to obtain ζ from z. Therefore, as announced above, the mapping problem can be reduced to repeated applications of a function, MAP, a sample coding of which is given in Fig. 8, regardless of the complexity of the geometry and of the direction in which the mapping is considered(from the physical cross section to the near-circle, or vice versa). In the calling sequence, INDEX is set equal to 1 if (9) is used to get ζ from z (in which case POINT means z and MAP means ζ), equal to -1 if (16) is used to get z from ζ (in which case POINT means ζ and MAP means z); FACTOR is any convenient number having the same sign as μ. The meaning and use of DER will be discussed later on. Note also that H(J,J) and POWER(J) are h and δ respectively as they appear in (9) and (16). Finally, note that in the program of Fig. 8 the special cases shown in Fig. 5 are not contemplated.

5. Examples

We turn now to examining few examples of mappings, involving non-trivial geometries. Note that the input is the geometry alone (which obviously includes the location of edges and corners in the physical plane).

The program orders the edges and corners in order of increasing δ, and finds the location of their images in the ζ-plane. Then, at regularly spaced values of θ between $-\pi/2$ and $\pi/2$, it finds, by trial and error (and using the mappings in reverse), which value of b produces a point on the original contour in the z-plane; generally, three iterations are sufficient. In these test cases, a shock is assumed as a circular boundary in the z-plane. Once more, by trial and error, all the proper values of $c(\theta)$ are found. Finally, for each θ, and for intermediate values of X, defined by

$$X = \left(\frac{\rho - b}{c - b}\right)^2 \tag{17}$$

the remaining points on the grid are determined. Note the slight difference between (17) and the first of (2), which permits grid lines to concentrate in the vicinity of the body. The figures are self-explanatory. In Fig. 9 the case of Fig. 7 is solved; in Fig. 10 we see a similar problem (with equal values of the corner angles) but with a more clustered geometry; in Fig. 11 a case similar to the one of Fig. 3a is considered (an airplane with a fin on the wing); and, finally, in Fig. 12 a cross section of a fuselage and an arrow wing is mapped. Note that in the latter case the near-circle contour is composed of alternating parts representing rigid walls and points in the free flow.

6. Coupling of Mappings and Equations of Motion

In non-dimensional form, let P be the logarithm of pressure, S the entropy, $\mathcal{T}$ the temperature, defined by

$$\mathcal{T} = \exp\left(\frac{\gamma - 1}{\gamma} P + \frac{1}{\gamma} S\right) \tag{18}$$

and $\vec{V}$ the velocity vector. The equations of motion are:

$$(19)\qquad \begin{cases} \vec{V}\cdot\nabla P + \gamma\nabla\cdot\vec{V} = 0 \\ \frac{1}{2}\nabla(\vec{V}^2) - \vec{V}\times\nabla\times\vec{V} + \mathcal{C}\nabla P = 0 \\ \vec{V}\cdot\nabla S = 0 \end{cases}$$

Let $\hat{I}, \hat{J}, \hat{K}$ be the unit vectors in the direction of the x-, y-, and t-axis, respectively. Let also $\hat{i}$ and $\hat{j}$ be the unit vectors in the z-plane, parallel to the θ=constant line and the ρ-constant line at each point. Let us denote by an index, $_1$, all vector operators defined in a t=constant plane only, and let

$$(20)\qquad \vec{V} = w(\vec{\chi} + \vec{K})$$

It is easy to prove that the equations of motion (19) can be recast in the form:

$$(21)\qquad \begin{cases} \left(1 - \frac{a^2}{w^2}\right) P_t + \vec{\chi}\cdot\nabla_1 P + \gamma\nabla_1\cdot\vec{\chi} = 0 \\ \frac{1}{2}\nabla_1(\vec{\chi}^2) - \vec{\chi}\times\nabla_1\times\vec{\chi} + \frac{\mathcal{C}}{w^2}(\nabla_1 P - P_t\vec{\chi}) + \vec{\chi}_t = 0 \\ \vec{\chi}\cdot\nabla_1 S + S_t = 0 \end{cases}$$

Scalar forms can be easily obtained from (21) but it must be kept in mind that, if non-Cartesian variables such as ρ and θ are used in each cross-sectional plane, the values of x and y at a node of the grid (at constant ρ and θ) change from plane to plane; therefore, for any function, $\mathcal{F}$:

$$(22)\qquad \mathcal{F}_t = \mathcal{F}_\tau + \mathcal{F}_\rho\,\rho_t + \mathcal{F}_\theta\,\theta_t$$

For example, if

$$(23)\qquad \vec{\chi} = \sigma\hat{i} + \eta\hat{y}$$

and

$$(24)\qquad g = \frac{d\zeta}{dz} = G\,e^{i\omega}$$

where ζ is the complex variable of the near-circle plane, obtained, if

necessary, through repeated applications of (9), it follows that

$$
(25)\qquad \begin{cases}
\nabla_1 \mathcal{F} = G\left(\mathcal{F}_\rho \hat{i} + \frac{1}{\rho}\mathcal{F}_\theta \hat{j}\right), \quad \vec{\chi}\cdot\nabla_1 \mathcal{F} = G\left(\sigma \mathcal{F}_\rho + \frac{\eta}{\rho}\mathcal{F}_\theta\right) \\
\vec{\chi} \times \nabla_1 \times \vec{\chi} = \frac{G^2}{\rho}\left[\left(\frac{\rho\eta}{G}\right)_\rho - \left(\frac{\sigma}{G}\right)_\theta\right](\eta\hat{i} - \sigma\hat{j}) \\
\nabla_1 \cdot \vec{\chi} = \frac{G^2}{\rho}\left[\left(\frac{\rho\sigma}{G}\right)_\rho + \left(\frac{\eta}{G}\right)_\theta\right] \\
\frac{1}{2}\nabla_1(\vec{\chi}^2) = G\left[(\sigma\sigma_\rho + \eta\eta_\rho)\hat{i} + \frac{1}{\rho}(\sigma\sigma_\theta + \eta\eta_\theta)\hat{j}\right] \\
\vec{\chi}_t = \left[\sigma_t + (\omega_t - \theta_t)\eta\right]\hat{i} + \left[\eta_t + (\theta_t - \omega_t)\sigma\right]\hat{j}
\end{cases}
$$

Let

$$
(26)\qquad f = f_1 + i f_2 = \frac{\partial \log \zeta}{\partial t}
$$

$$
(27)\qquad \varpi = \varpi_1 + i\varpi_2 = \zeta \frac{d \log g}{d\zeta} = \frac{\zeta}{g}\frac{d \log g}{dz}
$$

$$
(28)\qquad \psi = \psi_1 + i\psi_2 = \frac{\partial \log g}{\partial t}
$$

$$
(29)\qquad A_1 = G\frac{\sigma}{\chi} + \rho f_2, \quad A_2 = \frac{G}{\rho}\frac{\eta}{\chi} + f_2, \quad \left(\chi = 1 - \frac{a^2}{W^2}\right)
$$

$$
(30)\qquad B_1 = G\sigma + \rho f_1, \quad B_2 = \frac{G}{\rho}\eta + f_2
$$

$$
(31)\qquad D = \frac{G}{\rho}\left[\eta(1 - \varpi_1) - \sigma\varpi^2\right] + f_2 - \psi_2
$$

Then, (21) can be written in the form:

$$
(32)\qquad \begin{cases}
P_\tau + A_1 P_\rho + A_2 P_\theta + \frac{\gamma G}{\kappa}\left(\sigma_\rho + \frac{1}{\rho}\eta_\theta\right) + \frac{\gamma G}{\kappa\rho}\left[\sigma(1 - \varphi_1) + \eta\varphi_2\right] = 0 \\
\sigma_\tau + B_1\sigma_\rho + B_2\sigma_\theta + \frac{\mathcal{C}}{W^2}\left[-\sigma P_\tau + (G - \sigma\rho f_1)P_\rho - \sigma f_2 P_\theta\right] - \eta D = 0 \\
\eta_\tau + B_1\eta_\rho + B_2\eta_\theta + \frac{\mathcal{C}}{W^2}\left[-\eta P_\tau - \rho\eta f_1 P_\rho + \left(\frac{G}{\rho} - \eta f_2\right)P_\theta\right] + \sigma D = 0 \\
S_\tau + B_1 S_\rho + B_2 S_\theta = 0
\end{cases}
$$

A final change to the variables X, Y and T can now be performed but will not be considered in the present paper. As one can see by inspecting (32), prior to integrating the equations of motion one must evaluate g, f, φ, and ψ. In what follows, we will briefly expose how the evaluation is performed in a complicated case.

Let us assume that J successive mappings are necessary to eliminate all edges and corners, each partial mapping being of the form (9), that is:

$$\frac{z_{j+1}-1}{z_{j+1}+1} = \left(\frac{z_j - h_{jj}}{z_j + h_{jj}^*}\right)^{\delta_j} \qquad (j=1,2,\ldots,J) \tag{33}$$

We will also identify the physical z-plane with the z_1-plane. In such a plane we consider J+2 points, denoted by h_{j1} (Fig. 13); the first J points are representative of edges and corners and will operate as "hinges" in the successive mappings; the last two points are the intersection of the physical contour with the y-axis. The image of $h_{\ell 1}$ in the z_j-plane will be called $h_{\ell j}$. Note that h_{jj} is the active hinge in the j-th transformation and, therefore,

$$h_{j,j+1} = 1 \tag{34}$$

The J-th mapping produces a smooth contour, but it is convenient to have it as centered as possible about the origin of the ζ-plane. Therefore, a (J+1) st mapping is used, which is simply a translation:

$$\zeta = z_{J+1} - s\,, \quad s = \frac{1}{2}(h_{J+1,J+1} + h_{J+2,J+1}) \tag{35}$$

In conclusion,

$$\zeta = \zeta\left\{ z_{J+1} \langle z_J[\cdots z_2(z_1)]\rangle \right\}\,, \quad z_1 = z \tag{36}$$

For each partial mapping except (35), let

$$g_j = \frac{dz_{j+1}}{dz_j} = \frac{\delta_j \alpha_j (z_{j+1}^2 - 1)}{(z_j - h_{jj})(z_j + h_{jj}^*)} \tag{37}$$

where

$$h_{jj} = \alpha_j + i\beta_j \tag{38}$$

Then,

$$g = \frac{d\zeta}{dz} = \frac{dz_{J+1}}{dz_1} = \prod_{j=1}^{J} g_j \tag{39}$$

$$\varphi = \frac{\zeta}{g} \frac{d \log g}{dz} = \frac{\zeta}{g} \sum_{j=1}^{J} \frac{d \log g_j}{dz} = \frac{\zeta}{g} \sum_{j=1}^{J} \left(\frac{d \log g_j}{dz_j} \prod_{\ell=0}^{j-1} g_\ell \right)$$

$$= \frac{2\zeta}{g} \sum_{j=1}^{J} \frac{\prod_{\ell=0}^{j} g_\ell}{z_{j+1}^2 - 1} \left[z_{j+1} + \frac{1}{\delta_j} \left(\frac{h_{jj} - z_j}{\alpha_j} - 1 \right) \right] \tag{40}$$

$$(g_o = 1)$$

To evaluate f and ψ, let us observe first that

$$\frac{\partial z_{j+1}}{\partial \alpha_j} = -\delta_j \frac{(z_{j+1}^2 - 1)(z_j - i\beta_j)}{(z_j - h_{jj})(z_j + h_{jj}^*)} = g_j \left(\frac{h_{jj} - z_j}{\alpha_j} - 1 \right) \tag{41}$$

$$\frac{\partial z_{j+1}}{\partial \beta_j} = -ig_j \tag{42}$$

Then,

$$\frac{\partial z_{j+1}}{\partial \alpha_j} \frac{\partial \alpha_j}{\partial t} + \frac{\partial z_{j+1}}{\partial \beta_j} \frac{\partial \beta_j}{\partial t} = g_j \left(\frac{h_{jj} - z_j}{\alpha_j} \frac{\partial \alpha_j}{\partial t} - \frac{\partial h_{jj}}{\partial t} \right) \tag{43}$$

and

$$(44)\qquad \frac{\partial z_{j+1}}{\partial t} = g_j\left[\frac{\partial z_j}{\partial t} + \frac{h_{jj}-z_j}{\alpha_j}\frac{\partial \alpha_j}{\partial t} - \frac{\partial h_{jj}}{\partial t} + \frac{z_{j+1}^2-1}{2}\log\frac{z_j-h_{jj}}{z_j+h_{jj}^*}\frac{\partial \delta_j}{\partial t}\right]$$

Similarly,

$$(45)\qquad \frac{\partial \zeta}{\partial t} = \frac{\partial z_{J+1}}{\partial t} - \frac{1}{2}\left(\frac{\partial h_{J+1,J+1}}{\partial t} + \frac{\partial h_{J+2,J+1}}{\partial t}\right)$$

Note that $\partial h_{\ell,\,j+1}/\partial t$ can be computed as a particular case of (44):

$$(46)\qquad \frac{\partial h_{\ell,j+1}}{\partial t} = g_j\left[\frac{\partial h_{\ell j}}{\partial t} + \frac{h_{jj}-h_{\ell j}}{\alpha_j}\frac{\partial \alpha_j}{\partial t} - \frac{\partial h_{jj}}{\partial t} + \frac{h_{\ell,j+1}^2-1}{2}\log\frac{h_{\ell j}-h_{jj}}{h_{\ell j}+h_{jj}^*}\frac{\partial \delta_j}{\partial t}\right]$$

Note also that, if $\ell=j$, $\frac{\partial h_{j,\,j+1}}{\partial t} = 0$, a result consistent with (34).

The values of $\partial h_{\ell 1}/\partial t$ ($\ell=1, J+2$) and of $\partial \delta_j/\partial t$ are known from the geometry of the vehicle as a function of t. Therefore (46) permits all the values of $\partial h_{j+1,\,j+1}/\partial t$ (j=1 through J) to be computed recursively and (44) furnishes all the values of $\partial z_{j+1}/\partial t$, including $\partial z_{J+1}/\partial t$, in a similar way. Then, $\partial \zeta/\partial t$ is obtained from (45) and f is obviously equal to $\frac{1}{\zeta}\frac{\partial \zeta}{\partial t}$.

From Fig. 8 it appears that g_j, as defined by (37), is computed every time either $z_{j+1}(z_j)$ or $z_j(z_{j+1})$ is computed, and in either case it has the same meaning. The factor, g_j, appearing in (46), must be understood as

$$\frac{dh_{\ell,\,j+1}}{dh_{\ell,\,j}}$$

and is thus obtainable when MAP is applied to determine the values of $h_{\ell,\,j+1}$ from the values of $k_{\ell j}$.

Finally, to compute Ψ one uses (39) and (37) obtaining, after more manipulations,

$$(47)\quad \psi = \sum_{j=1}^{J} \frac{\partial \log g_j}{\partial t} = \sum_{j=1}^{J} \left[\frac{1}{\delta_j}\frac{\partial \delta_j}{\partial t} + \frac{1}{\alpha_j}\frac{\partial \alpha_j}{\partial t} + \frac{2 z_{j+1}}{z_{j+1}^2 - 1}\frac{\partial z_{j+1}}{\partial t} - 2\frac{(z_j - i\beta_j)\left(\frac{\partial z_j}{\partial t} - i\frac{\partial \beta_j}{\partial t}\right) - \alpha_j \frac{\partial \alpha_j}{\partial t}}{(z_j - h_{jj})(z_j + h_{jj}^*)} \right]$$

At this stage, all elements necessary to evaluate (47) numerically are available.

7. Conclusion

Sections 4 and 6 contain all the information which is necessary to use the conformal mapping concept, as explained in Section 3, for the numerical analysis of a three-dimensional, steady, supersonic, inviscid flow. Details of such analysis, from the fluid-mechanical viewpoint, and a sample calculation of a redimentary arrow-winged plane will be presented in a forthcoming Report.

References

1. Pandolfi, M.: Supersonic flow about elliptic cones with large semi-axis ratio, Report No. PP172, Istituto di Macchine, Politecnico di Torino, Dec. 1975.
2. Thompson, J.F., F.C. Thames, C.W. Martin and S.P. Shanks: Use of numerically generated body-fitted coordinate systems for solution of the Navier-Stokes equations, AIAA 2nd Comp. Fluid Dyn. Conf., Hartford, Conn., p. 68, June 1975.
3. Marconi, F. and M. Salas: Computation of three-dimensional flows about aircraft configurations, Comp. and Fluids, 1, p. 185, 1973.

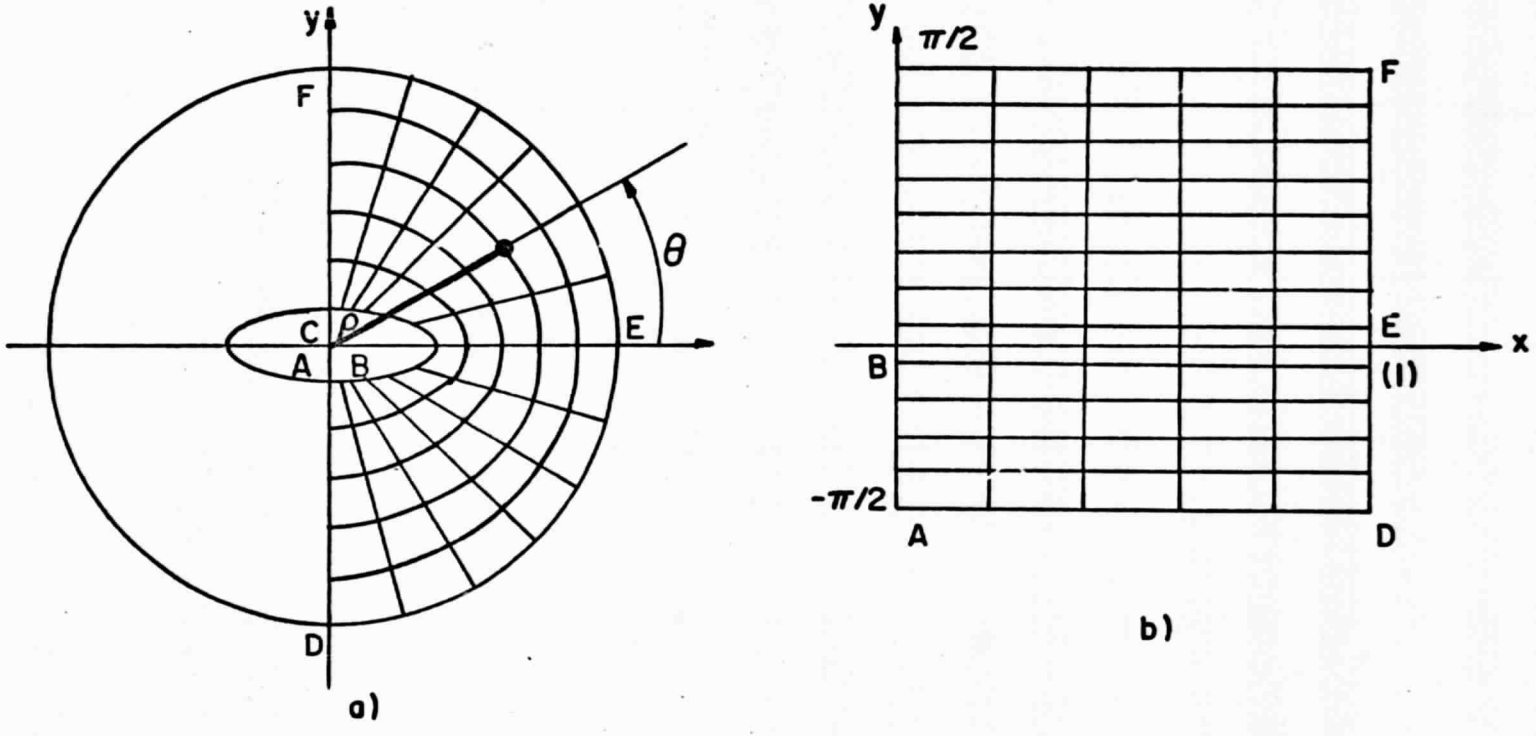

FIG. 1

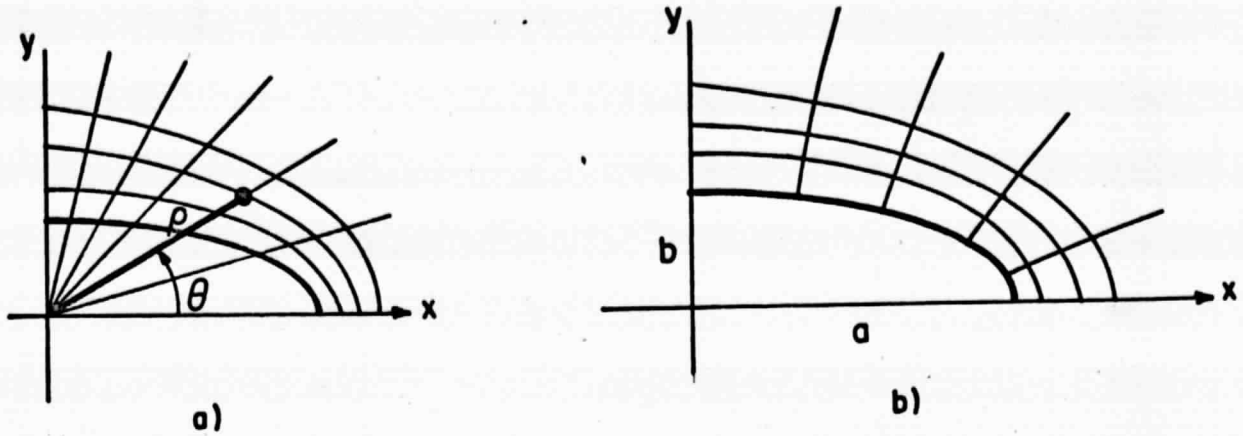

FIG. 2

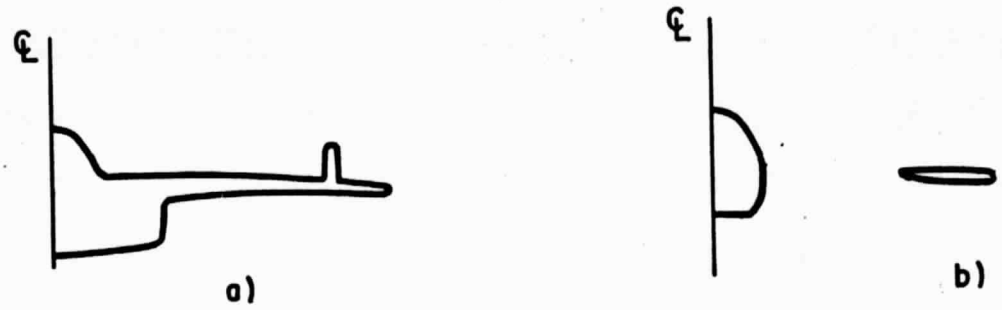

FIG. 3

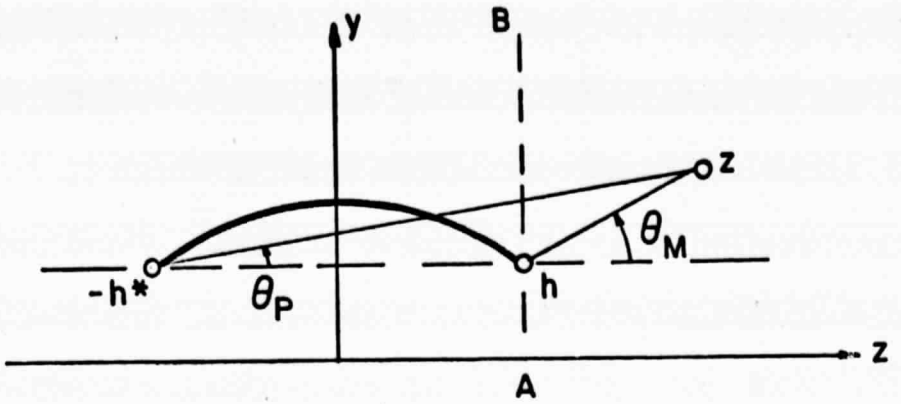

FIG. 4

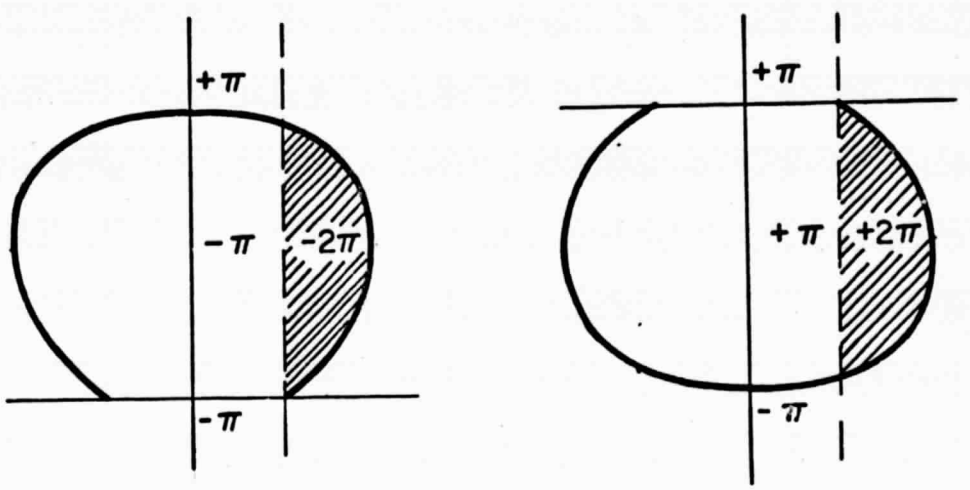

FIG.5

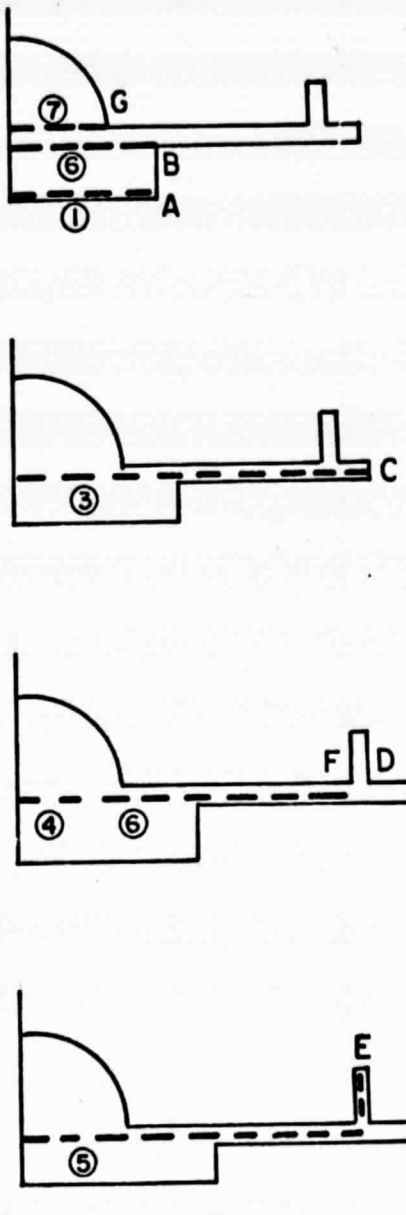

CUTS IN THE Z-PLANE

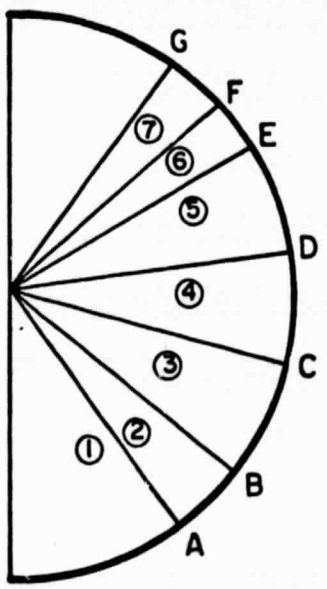

CUTS IN THE ζ-PLANE

FIG. 6

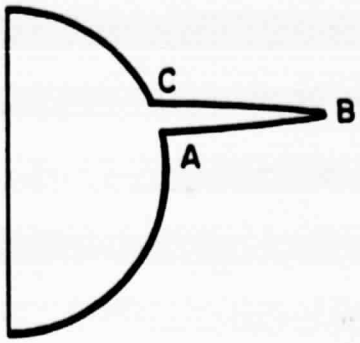

FIG. 7

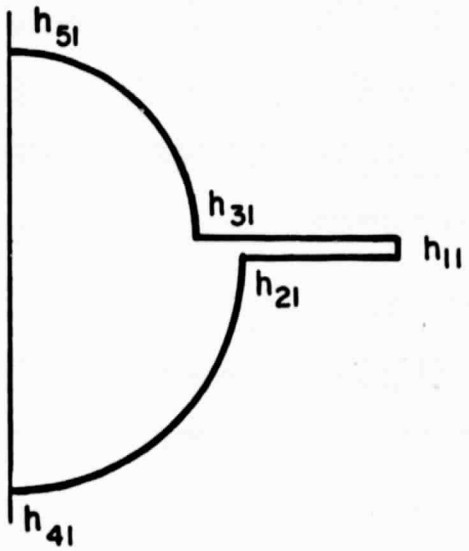

FIG. 13

```
      COMPLEX FUNCTION MAP(INDEX,J,POINT,FACTOR,DER)
      COMPLEX POINT,HINGE,CI,P,D,DER,H(10,10)
      COMMON/CMAP/PI,PI02,CI,H,POWER(10)
C     ****   DER IS DERIVATIVE  D(Z(J+1))/D(Z(J))    ****
      HINGE=H(J,J) $ POW=POWER(J) $ IF(INDEX.EQ.-1)POW=1./POW
      P=POINT $ D1=REAL(HINGE) $ D2=AIMAG(HINGE)
      IF(INDEX.EQ.1)P=(POINT-HINGE)/D1+1.
      XM=REAL(P)-1. $ YM=AIMAG(P) $ XP=XM+2.$ Y2=YM**2 $ RM2=XM**2+Y2
      RP2=XP**2+Y2 $ THP=ATAN(YM/XP) $ IF(XM.EQ.0.)GO TO 1
      THM=ATAN(YM/XM) $ IF(XM.GT.0.)GO TO 2 $ THM=THM+SIGN(PI,FACTOR)
      GO TO 2
    1 THM=SIGN(PI02,YM)
    2 D=(RM2/RP2)**(.5*POW)*CEXP(CI*POW*(THM-THP))
      MAP=(1.+D)/(1.-D) $ IF(INDEX.EQ.-1)GO TO 4
      DER=D1*POW*(MAP**2-1.)/((POINT-HINGE)*(POINT+CMPLX(D1,-D2)))
      RETURN
    4 MAP=HINGE+(MAP-1.)*D1
      DER=D1*(POINT**2-1.)/(POW*(MAP-HINGE)*(MAP+CMPLX(D1,-D2)))
      RETURN $ END
```

FIG. 8

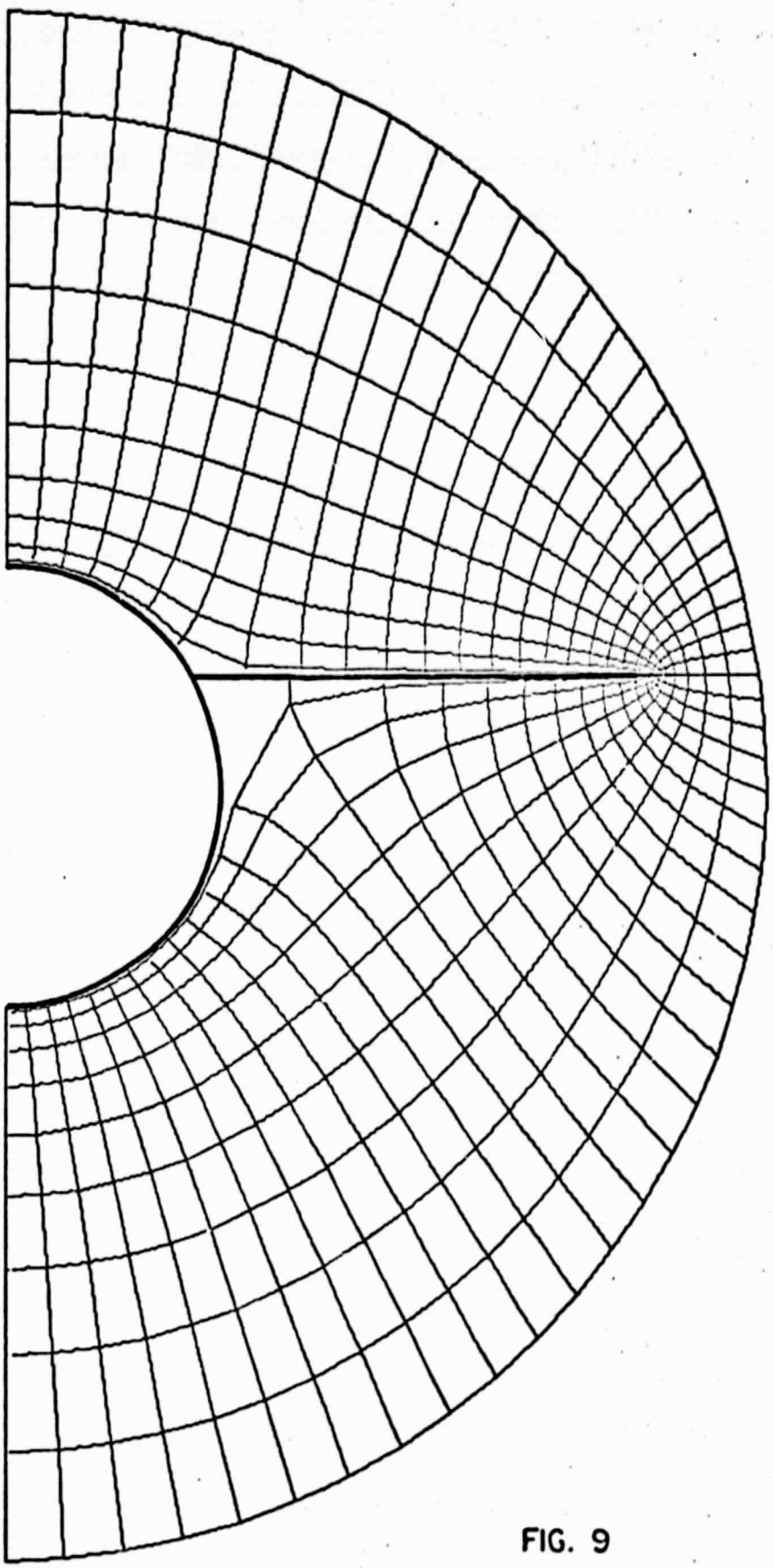

FIG. 9

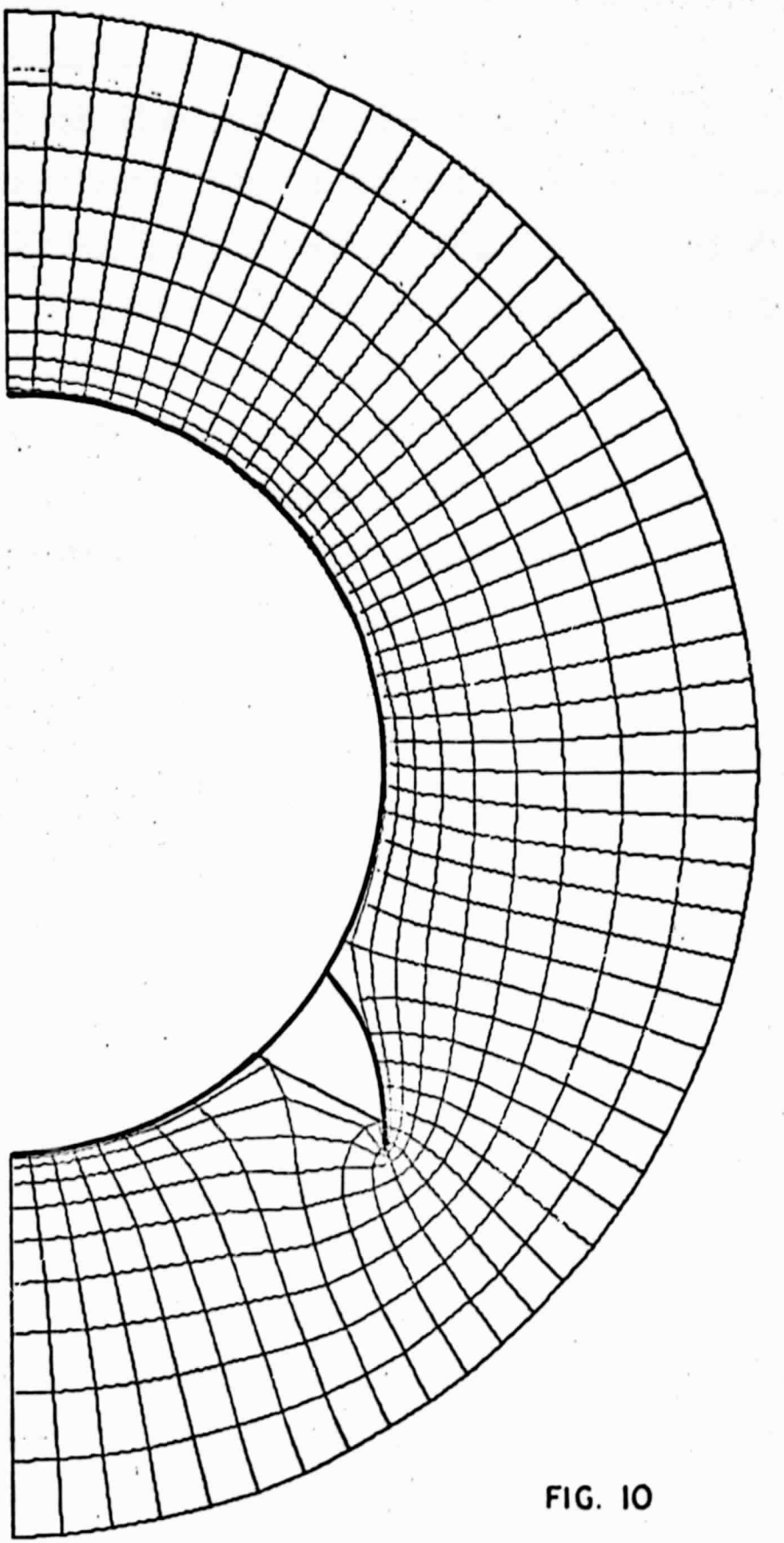

FIG. 10

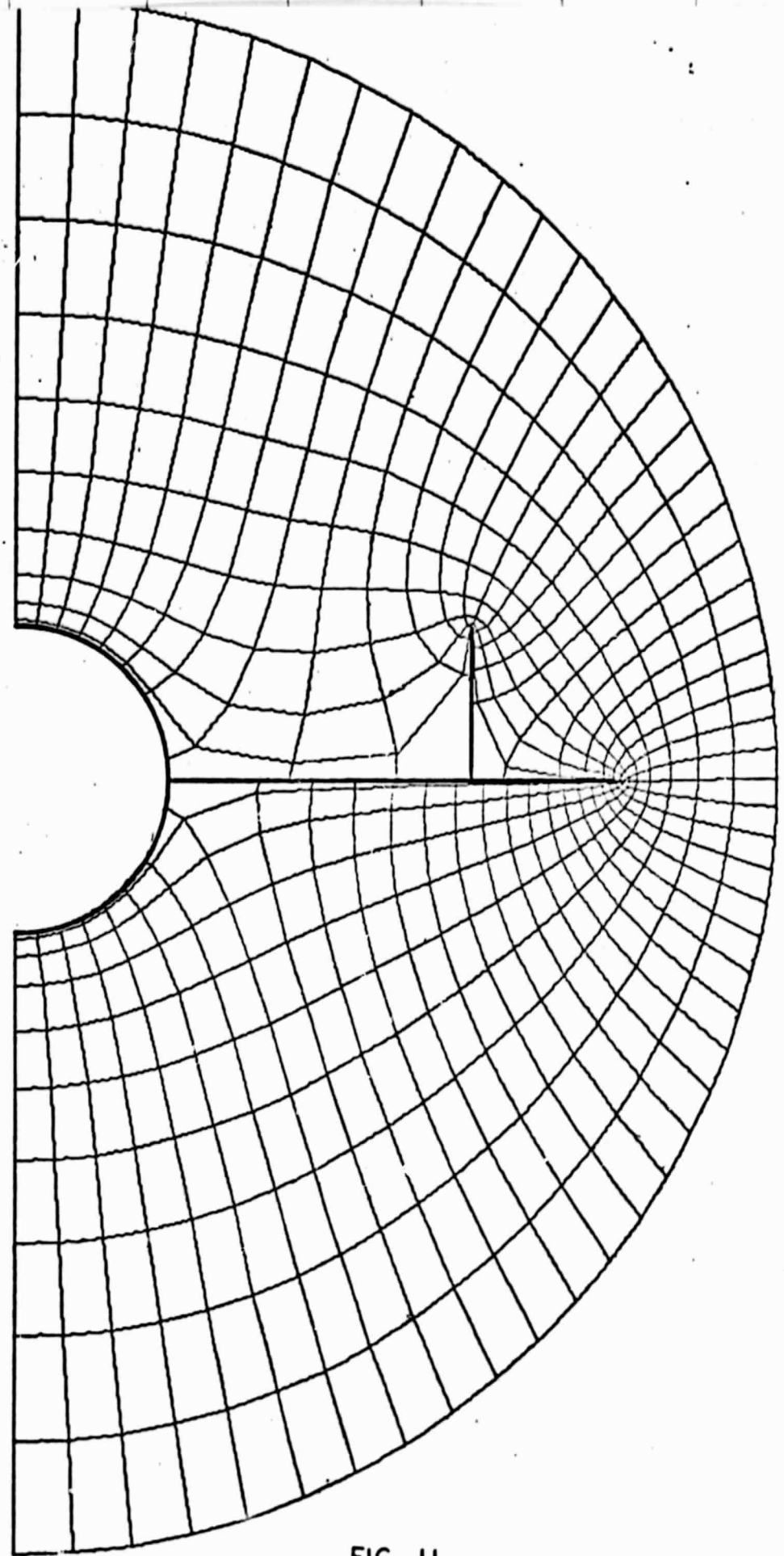

FIG. 11

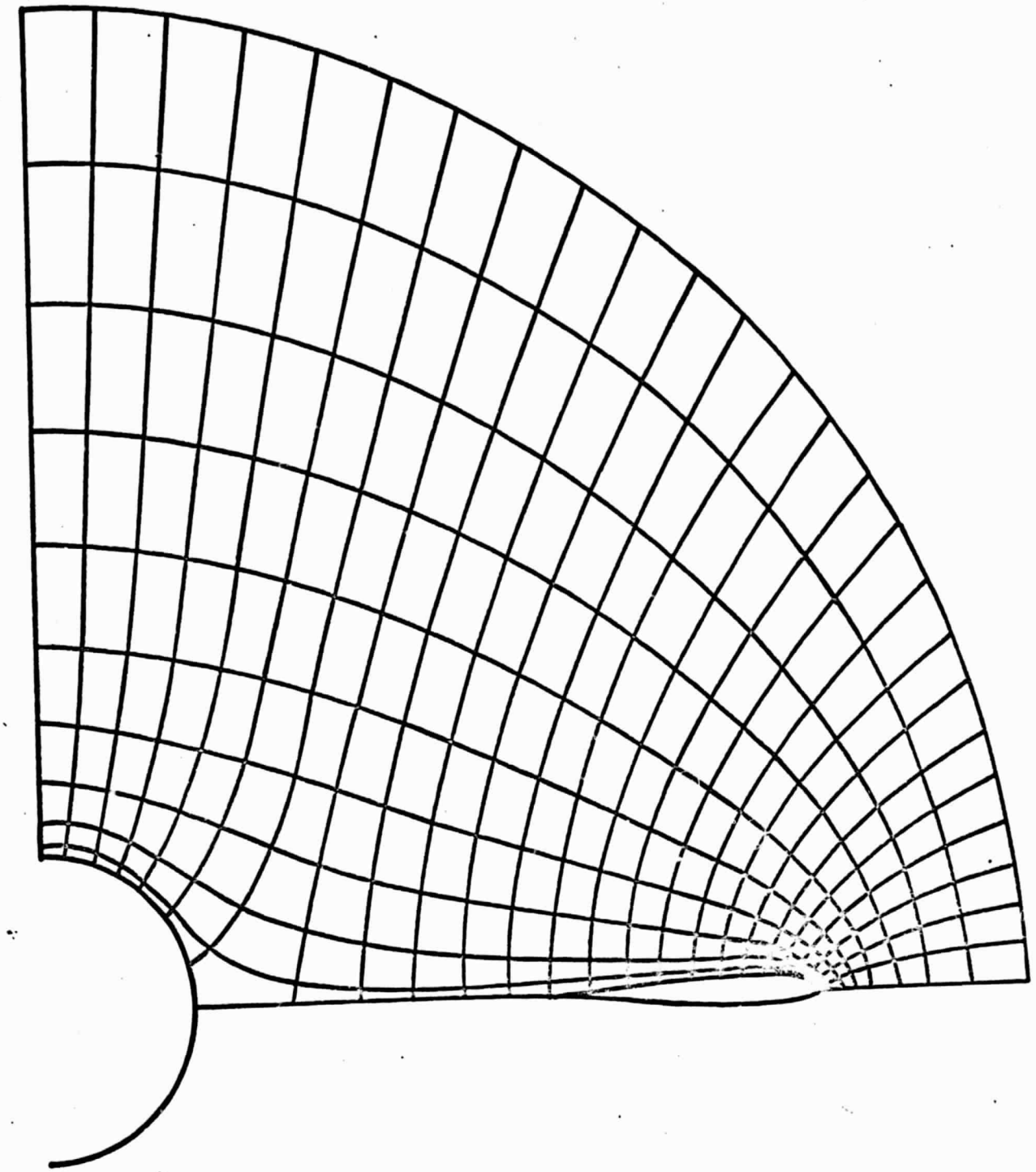

FIG. 12